

SHORT-RANGE CORRELATIONS AND THE ONE-BODY DENSITY MATRIX IN FINITE NUCLEI

A. Polls

*Departament d'Estructura i Constituents de la Matèria
Universitat de Barcelona
Diagonal 647, E-08028 Barcelona, Spain*

H. Mütter

*Institut für Theoretische Physik, Universität Tübingen,
Auf der Morgenstelle 14, D-72076 Tübingen, Germany*

W.H. Dickhoff

*Department of Physics, Washington University,
St. Louis, MO 63130, USA*

The effects of short-range correlations derived from a realistic meson-exchange potential on the single-particle density matrix in finite nuclei are investigated by analyzing the one-body density in terms of the natural orbits. Basic features of these natural orbits and their spectral distributions are discussed. For many observables it seems to be sufficient to approximate the one-body density matrix in terms of those natural orbits, which exhibit the largest occupation probabilities. For the investigation of the high-momentum components in the single-particle density, however, it is important to take into account natural orbits with small occupation probabilities, originating from the single-particle Green function at large negative energies.

I. INTRODUCTION

It is generally accepted that atomic nuclei are many-body systems in which correlations beyond the mean-field or Hartree-Fock picture play a significant role. Therefore it has always been a point of experimental and theoretical studies to find observables, which reflect these correlations in a unambiguous way. In this sense, the simultaneous study of density and momentum distributions in nuclei seems to be a sensitive test of nuclear models and may provide information on the correlations between the interacting nucleons [1]. Density and momentum distributions are one-body properties and therefore can be calculated from the single-particle spectral function which contains all the information on the single-particle structure of nuclei. Recent proton knock-out experiments employing the $(e, e'p)$ reaction have shown that correlations between nucleons are responsible for a reduction of the spectroscopic strength of valence hole states with respect to the uncorrelated mean-field values and for the fragmentation of the strength over a large excitation energy domain of the remaining nucleus [2–4].

The modern $(e, e'p)$ performed e.g. with the MAMI facility [4] in Mainz or at NIKHEF [3] in Amsterdam do not only provide information on the global spectroscopic strength but also yield results on the high-momentum components of the spectral function. The effects of correlations on the momentum and energy distribution of the single particle strength, in particular for these high momentum values, is presently a subject of discussion [5–10]. Most of the investigations have been performed for light nuclei [5–7] or infinite nuclear matter [11–17]. Results for heavier nuclei are typically derived from investigations of nuclear matter assuming a local density approximation [18–21].

A question that has attracted a lot of attention concerns the possibility of describing a given momentum distribution by means of an independent particle model. In the IPM the nucleus is considered to be a system of nucleons moving without residual interaction in a mean-field or single-particle potential. In this case the nuclear wave function is represented by a single Slater determinant. One way to clarify this point is by studying the natural orbits (no) [10,22–25]. These wave functions and their associated eigenvalues (n_α) (natural occupation numbers) are obtained by diagonalizing the one-body density matrix for the ground state of the A particle system. Therefore the one-body density matrix of the correlated system can be expressed in terms of these occupation numbers n_α and the corresponding natural orbits ϕ_α^{no} by

$$\rho(r, r') = \sum_{\alpha} n_{\alpha} \phi_{\alpha}^{no*}(r) \phi_{\alpha}^{no}(r') \quad (1)$$

As the one body density matrix is diagonal in the no representation, this basis appears to contain the most suitable single-particle wave functions for the calculation of the expectation value of a general one-body operator. In particular, if the total wave function of the system is a unique Slater determinant build with single-particle wave functions then

the natural orbits coincide with those wave functions and the natural occupations are equal to unity. The deviations of this ideal situation indicate the impossibility to obtain the one-body density matrix from a single Slater determinant. One can say that the effect of correlations in the calculation of one-body observables are smallest when using the *no* basis; for example, the depletion of the Fermi sea is smallest in this basis [10].

Performing a microscopic calculation of the one-body Green function for ^{16}O we have recently demonstrated [26,27] that the nucleon-nucleon correlations induced by the short-range and the tensor components of a realistic interaction [28] yield an enhancement of the momentum distribution at high momenta as compared to the Hartree-Fock description. This enhancement, however, is only obtained after integrating over all excitation energies of the $A - 1$ particle system. On the other hand, a momentum distribution very similar to the one derived in the Hartree-Fock approximation is observed if one restricts the energy integration to the states of lowest energy for each set of orbital angular momentum l and j . Does this imply that correlation effects are visible in $(e, e'p)$ experiments to the low-lying states in $A - 1$ nucleus only in terms of the spectroscopic factors, which are reduced as compared to the independent particle model? In order to discuss this question, we will analyze the results of the single-particle Green function obtained with the method described in [27] in terms of natural orbits and their occupation numbers. This analysis will also allow us to study the effects of correlations on the local density distribution $\rho(r)$ and other one-body observables in ^{16}O .

After this introduction, the techniques to evaluate the single-particle Green function, the density matrix and the natural orbits are briefly described in the next section. The discussion of our numerical results are presented in section 3 and the main conclusions of the work are summarized in the final section 4.

II. CALCULATION OF THE SINGLE PARTICLE DENSITY MATRIX

The aim of our investigation is the analysis of the single-particle density matrix ρ_{mn} , which is defined in a basis of appropriate single-particle states m, n by

$$\rho_{mn} = \langle \Psi_0^A | a_m^\dagger a_n | \Psi_0^A \rangle \quad (2)$$

where Ψ_0^A denotes the correlated ground state of the nucleus and a_m^\dagger (a_n) define the single-particle creation (annihilation) operators for the basis considered. For a nucleus like ^{16}O with a ground state of angular momentum $J = 0$ the density matrix can be separated into sub-matrices of given orbital angular momentum l , total angular momentum j and an isospin quantum number. In our discussion we will ignore the effects of the Coulomb interaction. This means that the results obtained in nuclei with $N = Z$ are identical for protons and neutrons and therefore we will drop the quantum number referring to the isospin. Using e.g. the momentum representation and performing a partial wave decomposition, the density matrix can be written as $\rho_{lj}(k_1, k_2)$, with lj referring to the “good” quantum numbers of angular momentum and k_1, k_2 define the absolute values of the momenta for the single-particle states m, n above.

Within the Green function approach [29] this density matrix can be evaluated from the imaginary part of the single-particle Green function by integrating

$$\rho_{lj}(k_1, k_2) = \int_{-\infty}^{\epsilon_F} dE \frac{1}{\pi} \text{Im} (g_{lj}(k_1, k_2; E)), \quad (3)$$

where the energy variable E corresponds to the energy difference between the ground state of the A particle system and the various energies of all the states in the $A - 1$ system (negative E with large absolute value correspond to high excitation energies in the remaining system) and ϵ_F is the Fermi energy.

The single-particle Green function g_{lj} or propagator is obtained from a solution of the Dyson equation

$$g_{lj}(k_1, k_2; E) = g_{lj}^{(0)}(k_1, k_2; E) + \int dk_3 \int dk_4 g_{lj}^{(0)}(k_1, k_3; E) \Delta \Sigma_{lj}(k_3, k_4; E) g_{lj}(k_4, k_2; E), \quad (4)$$

where $g^{(0)}$ refers to a Hartree-Fock propagator and $\Delta \Sigma_{lj}$ represents contributions to the real and imaginary part of the irreducible self-energy, which go beyond the Hartree-Fock approximation of the nucleon self-energy used to derive $g^{(0)}$. The definition and evaluation of the Hartree-Fock contribution as well as the calculation of $\Delta \Sigma$ will be discussed below.

The calculation of the self-energy is performed in terms of a G -matrix which is obtained as a solution of the Bethe-Goldstone equation for nuclear matter choosing for the bare NN interaction the One-Boson-Exchange potential B defined by Machleidt ([28], Tab.A.2). The Bethe-Goldstone equation has been solved for nuclear matter with a Fermi momentum $k_F = 1.4 \text{ fm}^{-1}$. This roughly corresponds to the saturation density of nuclear matter. The starting

energy has been chosen to be -10 MeV. The choices for the density of nuclear matter and the starting energy are rather arbitrary. It turns out, however, that the calculation of the Hartree-Fock term is not very sensitive to this choice [30]. Furthermore, we will correct this nuclear matter approximation by calculating the 2-particle 1-hole (2p1h) term displayed in Fig. 1b directly for the finite system, correcting the double-counting contained in the Hartree-Fock term (see discussion below).

Using vector bracket transformation coefficients [31], the G -matrix elements obtained from the Bethe-Goldstone equation can be transformed from the representation in coordinates of relative and center of mass momenta to the coordinates of single-particle momenta in the laboratory frame in which the 2-particle state would be described by quantum numbers such as

$$|k_1 l_1 j_1 k_2 l_2 j_2 J T\rangle, \quad (5)$$

where k_i , l_i and j_i refer to momentum and angular momenta of particle i whereas J and T define the total angular momentum and isospin of the two-particle state. It should be noted that Eq. (5) represents an antisymmetrized 2-particle state. Performing an integration over one of the k_i , one obtains a 2-particle state in a mixed representation of one particle in a bound harmonic oscillator while the other is in a plane wave state

$$|n_1 l_1 j_1 k_2 l_2 j_2 J T\rangle = \int_0^\infty dk_1 k_1^2 R_{n_1, l_1}(\alpha k_1) |k_1 l_1 j_1 k_2 l_2 j_2 J T\rangle .. \quad (6)$$

Here R_{n_1, l_1} stands for the radial oscillator function and the oscillator length $\alpha = 1.72 \text{ fm}^{-1}$ has been selected. This choice for the oscillator length corresponds to an oscillator energy of $\hbar\omega_{osc} = 14 \text{ MeV}$. Therefore the oscillator functions are quite appropriate to describe the wave functions of the bound single-particle states in ^{16}O . Indeed, it turns out that the single-particle wave functions determined in self-consistent BHF calculations for ^{16}O have a large overlap with these oscillator functions [32]. Using the nomenclature defined in Eqs. (5) - (6) our Hartree-Fock approximation for the self-energy is easily obtained in the momentum representation

$$\Sigma_{l_1 j_1}^{HF}(k_1, k'_1) = \frac{1}{2(2j_1 + 1)} \sum_{n_2 l_2 j_2 J T} (2J + 1)(2T + 1) \langle k_1 l_1 j_1 n_2 l_2 j_2 J T | G | k'_1 l_1 j_1 n_2 l_2 j_2 J T \rangle. \quad (7)$$

The summation over the oscillator quantum numbers is restricted to the states occupied in the IPM of ^{16}O . This Hartree-Fock part of the self-energy is real and does not depend on the energy. It should be noted that the approximation, which is called Hartree-Fock in this paper is not a Hartree-Fock approach in terms of the bare NN interaction V . Using a realistic NN interaction V , as it is done here, such a Hartree-Fock approach would yield a very unreasonable description, in which the nucleons are typically unbound [33]. What is called Hartree-Fock approximation here, is defined in terms of a nuclear matter G matrix, which accounts already for NN correlations.

In order to evaluate now the single-particle Green function and densities we consider a complete basis within a spherical box of a radius R_{box} . This box radius should be larger than the radius of the nucleus considered. The calculated observables are independent of the choice of R_{box} , if it is chosen to be around 15 fm or larger. A complete and orthonormal set of regular basis functions within this box is given by

$$\Phi_{iljm}(\mathbf{r}) = \langle \mathbf{r} | k_i l j m \rangle = N_{il} j_l(k_i r) \mathcal{Y}_{l j m}(\theta \phi) \quad (8)$$

In this equation $\mathcal{Y}_{l j m}$ represent the spherical harmonics including the spin degrees of freedom and j_l denote the spherical Bessel functions for the discrete momenta k_i which fulfill

$$j_l(k_i R_{\text{box}}) = 0. \quad (9)$$

Using the normalization constants

$$N_{il} = \begin{cases} \frac{\sqrt{2}}{\sqrt{R_{\text{box}}^3} j_{l-1}(k_i R_{\text{box}})}, & \text{for } l > 0 \\ \frac{i\pi\sqrt{2}}{\sqrt{R_{\text{box}}^3}}, & \text{for } l = 0, \end{cases} \quad (10)$$

the basis functions defined in Eq. (8) are orthogonal and normalized within the box

$$\int_0^{R_{\text{box}}} d^3 r \langle k_i' l' j' m' | \mathbf{r} \rangle \langle \mathbf{r} | k_i l j m \rangle = \delta_{ii'} \delta_{ll'} \delta_{jj'} \delta_{mm'}. \quad (11)$$

Note that the basis functions defined for discrete values of the momentum k_i within the box differ from the plane wave states defined in the continuum with the corresponding momentum just by the normalization constant, which is $\sqrt{2/\pi}$ for the latter. This enables us to determine the matrix elements of the nucleon self-energy in the basis of Eq. (8) from the results presented in Eq. (7). For that purpose the Hartree-Fock Hamiltonian is diagonalized

$$\sum_{n=1}^{N_{\max}} \langle k_i | \frac{k_i^2}{2m} \delta_{in} + \Sigma_{lj}^{HF} | k_n \rangle \langle k_n | a \rangle_{lj} = \epsilon_{alj}^{HF} \langle k_i | a \rangle_{lj}. \quad (12)$$

Here and in the following the set of basis states in the box has been truncated by assuming an appropriate N_{\max} . In the basis of Hartree-Fock states $|a\rangle$, the Hartree-Fock propagator is diagonal and given by

$$g_{ij}^{(0)}(a; E) = \frac{1}{E - \epsilon_{alj}^{HF} \pm i\eta}, \quad (13)$$

where the sign in front of the infinitesimal imaginary quantity $i\eta$ is positive (negative) if ϵ_{alj}^{HF} is above (below) the Fermi energy. Knowing the expansion coefficients of the Hartree-Fock states in the ‘‘box-basis’’ $\langle k_i | a \rangle_{lj}$ it is of course trivial to present $g_{ij}^{(0)}$ in the basis of Eq. (8).

The contributions to the self-energy, which are of second order in the nuclear matter G matrix are represented by the diagrams displayed in Figs. 1b) and 1c), referring to intermediate 2p1h and 2-hole 1-particle (2h1p) states, respectively. These two contributions define the correction to the self-energy $\Delta\Sigma$ beyond the Hartree-Fock approximation in the Dyson Eq. (4). These two contributions yield a complex and energy-dependent correction to the self-energy. The 2p1h contribution to the imaginary part is given by

$$\begin{aligned} W_{l_1 j_1}^{2p1h}(k_1, k'_1; E) &= \frac{-1}{2(2j_1+1)} \sum_{n_2 l_2 j_2} \sum_{l_3 l_4 j_3 j_4} \sum_{JT} \int k_3^2 dk_3 \int k_4^2 dk_4 (2J+1)(2T+1) \\ &\quad \times \langle k_1 l_1 j_1 n_2 l_2 j_2 JT | G | k_3 l_3 j_3 k_4 l_4 j_4 JT \rangle \\ &\quad \times \langle k_3 l_3 j_3 k_4 l_4 j_4 T | G | k'_1 l_1 j_1 n_2 l_2 j_2 JT \rangle \\ &\quad \times \pi \delta \left(E + \epsilon_{n_2 l_2 j_2} - \frac{k_3^2}{2m} - \frac{k_4^2}{2m} \right), \end{aligned} \quad (14)$$

where the ‘‘experimental’’ single-particle energies $\epsilon_{n_2 l_2 j_2}$ are used for the hole states (-47 MeV, -21.8 MeV, -15.7 MeV for $s_{1/2}$, $p_{3/2}$ and $p_{1/2}$ states, respectively), while the energies of the particle states are given in terms of the kinetic energy only. The expression in Eq. (14) still ignores the requirement that the intermediate particle states must be orthogonal to the hole states, which are occupied for the nucleus under consideration. The techniques to incorporate the orthogonalization of the intermediate plane wave states to the occupied hole states as discussed in detail by Borromeo et al. [34] have also been used here. The 2h1p contribution to the imaginary part $W_{l_1 j_1}^{2h1p}(k_1, k'_1; E)$ can be calculated in a similar way (see also [34]).

Our choice to assume pure kinetic energies for the particle states in calculating the imaginary parts of W^{2p1h} (Eq. (14)) and W^{2h1p} may not be very realistic for the excitation modes at low energy. Indeed a sizeable imaginary part in W^{2h1p} is obtained only for energies E below -40 MeV. As we are mainly interested, however, in the effects of short-range correlations, which lead to excitations of particle states with high momentum, the choice seems to be appropriate. A different approach would be required to treat the coupling to the very low-lying two-particle-one-hole and two-hole-one-particle states in an adequate way. Attempts at such a treatment can be found in Refs. [35–38].

The real parts of the 2p1h and 2h1p terms in the self-energy can be calculated from the corresponding imaginary parts by using dispersion relations [10]. As an example we present the dispersion relation for the 2p1h part, which is given by

$$V_{l_1 j_1}^{2p1h}(k_1, k'_1; E) = \frac{P}{\pi} \int_{-\infty}^{\infty} \frac{W_{l_1 j_1}^{2p1h}(k_1, k'_1; E')}{E' - E} dE', \quad (15)$$

where P means a principal value integral. Since the Hartree-Fock contribution Σ^{HF} has been calculated in terms of a nuclear matter G -matrix, it already contains 2p1h terms of the kind displayed in Fig. 1b). Therefore one would run into problems of double counting if one simply adds the real part V^{2p1h} to the Hartree-Fock self-energy. Notice that Σ^{HF} does not contain any imaginary part because it is calculated with a nuclear matter G -matrix at a starting energy for which G is real. In order to avoid such an over counting of the particle-particle ladder terms, we subtract from the real part of the self-energy a correction term V_c , which just contains this contribution calculated in nuclear matter [27].

Summing up the various contributions we obtain the following expression for the correction to the Hartree-Fock self-energy

$$\Delta\Sigma = (V^{2p1h} - V_c + V^{2h1p}) + i(W^{2p1h} + W^{2h1p}). \quad (16)$$

Rather than calculating the various contributions to $\Delta\Sigma$ in the basis of plane wave states, one may also calculate $\Delta\Sigma$ in the box basis defined in Eq. (8) or in the basis of Hartree-Fock states a, b , which we have obtained from the diagonalization in Eq. (12). In this basis it is easy to determine the so-called reducible self-energy, originating from an iteration of $\Delta\Sigma$, by solving

$$\langle a | \Sigma_{lj}^{red}(E) | b \rangle = \langle a | \Delta\Sigma_{lj}(E) | b \rangle + \sum_c \langle a | \Delta\Sigma_{lj}(E) | c \rangle g_{lj}^{(0)}(c; E) \langle c | \Sigma_{lj}^{red}(E) | b \rangle \quad (17)$$

and obtain the propagator, which corresponds to the solution of the Dyson Eq. (4) from

$$g_{lj}(a, b; E) = g_{lj}^{(0)}(a; E) \langle a | \Sigma_{lj}^{red}(E) | b \rangle g_{lj}^{(0)}(b; E). \quad (18)$$

Using this representation of the Green function one can calculate the continuum contribution to the density matrix in the “box basis” from

$$\rho_{lj}^c(k_1, k_2) = \frac{1}{\pi} \int_{-\infty}^{E_{2h1p}} dE \operatorname{Im} \left(\sum_{a,b} \langle k_1 | a \rangle_{lj} g_{lj}(a, b; E) \langle b | k_2 \rangle_{lj} \right), \quad (19)$$

where the integration limit E_{2h1p} refers to the negative threshold of 2h1p states for the lj combination considered. In our studies this energy is well below the corresponding Hartree-Fock energies. Therefore the imaginary part of g_{lj} in the region of integration is different from zero only due to the imaginary part in Σ^{red} , which just describes the coupling of the quasi particle states to the 2h1p continuum.

Besides this continuum contribution, the hole spectral function also receives contributions from the quasihole states [29]. The energies and wave functions of these quasihole states can be determined by diagonalizing the Hartree-Fock Hamiltonian plus $\Delta\Sigma$ in the “box basis”

$$\sum_{n=1}^{N_{\max}} \langle k_i | \frac{k_i^2}{2m} \delta_{in} + \Sigma_{lj}^{HF} + \Delta\Sigma_{lj}(E = \epsilon_{\Upsilon lj}^{qh}) | k_n \rangle \langle k_n | \Upsilon \rangle_{lj} = \epsilon_{\Upsilon lj}^{qh} \langle k_i | \Upsilon \rangle_{lj}. \quad (20)$$

Since in the present work $\Delta\Sigma$ only contains a sizeable imaginary part for energies E below ϵ_{Υ}^{qh} , the energies of the quasihole states come out real and the continuum contribution is separated in energy from the quasihole contribution. The quasihole contribution to the density matrix is given by

$$\rho_{\Upsilon lj}^{qh}(k_1, k_2) = Z_{\Upsilon lj} \langle k_1 | \Upsilon \rangle_{lj} \langle \Upsilon | k_2 \rangle_{lj}, \quad (21)$$

with the spectroscopic factor for the quasihole state given by [29]

$$Z_{\Upsilon lj} = \left(1 - \frac{\partial \langle \Upsilon | \Delta\Sigma_{lj}(E) | \Upsilon \rangle}{\partial E} \Big|_{\epsilon_{\Upsilon lj}^{qh}} \right)^{-1}. \quad (22)$$

Finally, the total single-particle density matrix is given as the sum of the continuum part of Eq. (19) and the quasihole contributions of Eq. (21) summed over all quasihole states with an energy below the Fermi energy ϵ_F

$$\rho_{lj}(k_1, k_2) = \rho_{lj}^c(k_1, k_2) + \sum_{\epsilon_{\Upsilon lj}^{qh} < \epsilon_F} \rho_{\Upsilon lj}^{qh}(k_1, k_2). \quad (23)$$

At this stage it is now of course straightforward to determine the natural orbits and their occupation numbers by diagonalizing this density matrix according to Eq. (1).

III. RESULTS AND DISCUSSION

A. Natural orbits and occupations

The numerical results to be discussed in this section have been obtained for each combination of orbital angular momentum l and total angular momentum j by using a basis of single-particle states defined according to Eqs. (8) - (10) for a spherical box with a radius R of 20 fm. Basis states up to $N_{\max}=20$ were taken into account. With these assumptions the density matrix for each single-particle channel lj is represented by a matrix of dimension $N_{\max}=20$. The diagonalization of these matrices yields eigenvalues which are the occupation probabilities $n_{lj\alpha}$ of the natural orbits (see Eq.(1)) and the eigenvectors correspond to the expansion coefficients of these natural orbits ($\phi_{lj\alpha}$) in the chosen basis.

Results for these occupation probabilities are displayed in table I ordered for each partial wave (lj) according to the magnitude of the occupation probability. Here and in the following we will use the notation that the natural orbit identified by $\alpha=1$ corresponds to the orbit with largest occupation probability and also the orbits with $\alpha=2\dots 20$ are ordered with respect to the occupation probability n_{α} . Note that natural orbits with α larger than 4 show an occupation which is so close to zero, that their contribution to the total occupations for each lj , which are also given in table I, is hardly visible within the accuracy used in that table.

For those partial waves lj , for which one orbit is completely occupied in the Hartree-Fock (HF) approach ($s_{1/2}$, $p_{3/2}$, and $p_{1/2}$ in our example ^{16}O), one finds that the first natural orbit ($\alpha=1$) exhibits an occupation probability very close to one, while the occupation probabilities of the natural orbits for $\alpha=2$ and larger are smaller by about a factor of 0.01. Similar observations have been reported for the natural orbits of ^3He drops containing 70 atoms. [39] It is interesting to observe that the eigenvalues for the ‘occupied’ orbits in [39] are in general 10-40% smaller than the corresponding ones calculated here for ^{16}O , indicating that correlations between ^3He atoms are stronger than those between nucleons. For those orbits lj which are completely unoccupied in the HF approach, like $d_{5/2}$, $d_{3/2}$ or $f_{7/2}$ in our example, the occupation probabilities are of course much smaller in agreement with the results in [39]. The ratio $n_{\alpha=2}$ versus $n_{\alpha=1}$ for these orbits is not as small as in the case of the orbits with occupation in the HF approach. As we will discuss more in detail below, this difference is due to the quasihole contribution to the density in these “occupied” orbits, which is missing in the lj channels which don’t show any occupation in HF.

The total occupation of these orbits with $l > 1$ is decreasing with increasing l . This could be interpreted to reflect the feature that orbits which have a larger excitation energy within the shell-model are less occupied. It is remarkable, however, that for a given l the states with $j = l - 1/2$ are more populated than those with $j = l + 1/2$, although the spin-orbit term of the shell-model yields less binding for the former than for the latter states. This is true for the example of the d states displayed in the table but also for states with $l > 2$, which are not given explicitly here. In order to understand this feature we must recall that the occupation probability for e.g. natural orbits with $d_{5/2}$ symmetry in ^{16}O , reflects the probability to generate in knock-out reactions states of the $A - 1$ particle system

$$|\Psi_{lj}^{(A-1)}\rangle \leftarrow a_{lj} |\Psi_0^{(A)}\rangle . \quad (24)$$

The resulting state $|\Psi_{lj}^{(A-1)}\rangle$ is a one-hole state with respect to the correlated ground state of ^{16}O , it does not contain, however, any component with one hole in the $d_{5/2}$ orbit with respect to the HF ground state configuration for ^{16}O . Such configurations do not exist or do not have the particle number $(A - 1)=15$. The occupation probability of natural orbits with $d_{5/2}$ symmetry reflects the possibility of generating states with two-hole 1-particle or more complicate $(n+1)$ -hole n -particle configurations as compared to the HF ground state configuration for ^{16}O . This probability, however, is not affected by single-particle energies of the $d_{5/2}$ orbits but rather determined by the number and energies of these $(n+1)$ -hole n -particle configurations and the probability of these configurations to be generated by applying a_{lj} to the correlated ground state $|\Psi_0^{(A)}\rangle$. Keeping this in mind the occupation probabilities of the natural orbits with $l > 1$ are easily understood.

The radial shapes of natural orbits with $\alpha=1$ to 3 are displayed in Fig. 2. At first sight these natural orbits look like solutions of a Schrödinger equation for a particle moving in a single-particle potential. They exhibit the same l -dependence ($\phi_{lj\alpha} \sim r^l$) for small values of r , the number of nodes is essentially identical to $\alpha - 1$, and their values decrease for large distances as it is the case for single-particle wave functions for bound states.

In order to characterize these natural orbits with different α on a more quantitative level, we have calculated the square radii of these orbits

$$\langle r^2 \rangle_{lj\alpha} = \int r^2 dr \phi_{lj\alpha}^2(r) r^2 \quad (25)$$

and show some typical results in table II. It should be emphasized that the resulting $\langle r^2 \rangle_{lj\alpha}$ do not increase with the number of nodes, i.e. the value of α , as one expects from single-particle wave functions in a potential. Assuming e.g. an oscillator potential the corresponding values for $\langle r^2 \rangle$ increase as a function of α proportional to $(2\alpha+l-1/2)$. The results for the natural orbits are much less increasing with α , in the case of the $l = 1$ orbits the values obtained for $\alpha = 2$ are even smaller than the corresponding results for $\alpha = 1$. This means that the natural orbits with $\alpha > 1$ yield a density distribution much more localized in the center of the nucleus than would be obtained from corresponding single-particle wave functions for a local potential.

Furthermore it is remarkable that the values of $\langle r^2 \rangle$ obtained for the $\alpha = 1$ natural orbits with angular momenta $l = 2$ and $l = 3$ are smaller than the radii calculated for the natural orbits with large occupation probability and $l = 1$. This difference is due to the fact that the $l = 1$, $\alpha = 1$ natural orbits are dominated by the quasihole contribution to the density matrix (see Eq. 21). The quasihole wave functions have overlaps larger than 0.99 with the corresponding natural orbits $\alpha = 1$. The quasihole states contribute an occupation of 0.78, 0.914 and 0.898 to the total occupations of 0.921, 0.947 and 0.93 for the $\alpha = 1$ natural orbits with l_j equal to $s_{1/2}$, $p_{3/2}$ and $p_{1/2}$, respectively. The radii of the quasihole states are slightly larger than the radii of the corresponding natural orbits (see table II and also figure 3). This indicates that the continuum contribution to the natural orbits tend to have smaller radii than the quasihole part. Therefore it can also be understood that radii of natural orbits with $l > 1$, which do not contain any quasihole contributions, can be smaller than those for $l = 1$.

From a more general point of view, however, one may say that for all those orbits, which are occupied within the naive shell-model and therefore yield a quasihole state, the radial wave function for the natural orbit with largest occupation probability ($\alpha = 1$) is very similar to the wave function of the quasihole state. Furthermore, both wave functions are very close to the corresponding single-particle wave functions obtained in the HF approach (see figure 3).

Summarizing this part of the discussion we find that for a given lj the continuum contribution to the density matrix (see Eq. 19) yields smaller radii than the corresponding quasihole wave function. Even if we sum the contributions of all natural orbits

$$\langle r^2 \rangle_{lj} = \frac{\sum_{\alpha} n_{lj\alpha} \langle r^2 \rangle_{lj\alpha}}{\sum_{\alpha} n_{lj\alpha}} \quad (26)$$

the result is smaller than just the radius of the quasihole state (see table II). In order to obtain the total radius of the nucleus one has to sum over all partial waves lj , multiply each $\langle r^2 \rangle_{lj}$ by the total occupation of these orbits $\sum_{\alpha} n_{lj\alpha}$ times the degeneracy $(2(2j+1))$ and divide by the total particle number. Due to the depletion of states with $l \leq 1$ accompanied by a small occupation of orbits with $l > 1$ one obtains a value for the total radius ($R=2.55$ fm), which is only slightly below the result obtained in the Hartree-Fock approach ($R=2.59$ fm).

These features are also displayed in figure 4, where the local density distribution obtained in HF (long dashes) is compared to the total density distribution (solid line). Also we present the contribution to the total density distribution coming from partial waves with $l > 1$ (short dashes). One finds that the depletion of states with small l (in particular $l = 0$) yields a reduction of the density in the center of the nucleus. The difference between the density distribution from the quasi-hole approximation (dashed-dotted line) and the total result is due to the continuum contribution to the density.

B. Spectral decomposition

In the preceding discussion it has been pointed out already that the natural orbits with occupation probabilities close to one are dominated by the quasihole contribution. This means that features of these natural orbits are explored in knock-out experiments like $(e, e'p)$ populating the states of low energy in the daughter nucleus. In the following we would like to discuss the question, to which extent the analysis of experiments with large missing energies, leading to high excitation energies in the residual $(A - 1)$ system, exhibits the properties of the natural orbits with smaller occupation probabilities.

For that purpose we analyze the continuum contribution to the density matrix (ρ^c , see eq.(19)). For the example of orbits with $l = 0$, the largest occupation numbers resulting from the diagonalization of this continuum part of the density matrix are listed in table III and the corresponding natural orbits are displayed in figure 5. The natural orbit with largest occupation, obtained from this continuum part of the density matrix, yields a radial wave function, which is again very similar to the corresponding quasihole state. In fact, the overlap of the natural orbit displayed in the left part of figure 5 has an overlap with the quasihole wave function of the $l = 0$ state, which is as large as 0.997. This means that also the continuum part of the density matrix is characterized by a dominant natural orbit very similar to the quasihole state.

In a next step we split the energy integration of eq.(19) into 2 parts. The first interval ranges from $E = -100$ MeV to the threshold of the $2h1p$ continuum, while the second interval covers energies from $-\infty$ to $E = -100$ MeV. Restricting the energy integration to one of these two intervals we can study either the single-particle density to be observed in knock-out experiments with very large missing energies (interval 2) or at medium missing energies. Eigenvalues (i.e. occupation probabilities n_α) and eigenvectors (natural orbits) of these parts of the density matrix are also presented in table III and figure 5, respectively.

The natural orbits originating from the energy interval 2 (large missing energies) are more localized in the center of the nucleus than those derived from the energy interval which corresponds to lower excitation energies in the residual system. The overlaps of the various natural orbits with the same α , however, are still large (typically larger than 0.95). What seems to be more significant is the relative importance of the different energy intervals for the various natural orbits. The occupation of the $\alpha = 1$ natural orbit mainly originates from the energy interval 1, whereas the natural orbits with α equal to 2 or larger, collect the main part of the occupation from energies below -100 MeV in the integral of eq.(19).

The same features are also observed in the other partial waves as can be seen from the results displayed in table IV. In this table we give for various partial waves lj the occupation probabilities of the natural orbits derived from the total density matrix, split into the contribution resulting from the quasihole part of the density matrix (denoted by n_α^{qh}) and the continuum part (n_α^c). These results show again that the $\alpha = 1$ natural orbits are dominated by the quasihole component of the density matrix, while the other natural orbits mainly originate from the continuum contribution to the single-particle density.

Furthermore we have listed for each natural orbit, $\phi_{lj\alpha}$, the mean value for the energy in the $2h1p$ continuum (see also Eq.(19))

$$\omega_{lj\alpha} = \frac{1}{\pi n_\alpha^c} \int_{-\infty}^{E_{2h1p}} dE E \text{Im} \left(\sum_{k_1, k_2} \langle \alpha | k_1 \rangle_{lj} g_{lj}(k_1, k_2; E) \langle k_2 | \alpha \rangle_{lj} \right). \quad (27)$$

In this equation $g_{lj}(k_1, k_2; E)$ stands for the single-particle Green function in the “box-basis” of Eqs.(8) - (10) and $\langle k_i | \alpha \rangle_{lj}$ denote the expansion coefficients of the natural orbits in this basis.

Inspecting these mean values for the energies one finds that the absolute values of these energies increase with α , the index of the natural orbits chosen with respect to the occupation probability. This implies that the natural orbits, which have radial wave functions with a larger number of nodes ($\alpha > 1$, see figure 2), “collect” the occupation at more negative energies than the natural orbits with $\alpha = 1$.

Also we list in table IV the continuum contribution to the expectation values for the kinetic energies of the natural orbits

$$t_{lj\alpha} = \frac{1}{\pi n_\alpha^c} \int_{-\infty}^{E_{2h1p}} dE \langle k_1 | T_{kin} | k_2 \rangle_{lj} \text{Im} \left(\sum_{k_1, k_2} \langle \alpha | k_1 \rangle_{lj} g_{lj}(k_1, k_2; E) \langle k_2 | \alpha \rangle_{lj} \right). \quad (28)$$

Also the expectation values $t_{lj\alpha}$ increase with α . For $\alpha=1$ they are slightly larger than the corresponding expectation values for the quasihole states. This is in line with the observation made above that the continuum part of the density matrix tends to decrease the radius of the natural orbit with $\alpha = 1$ as compared to the quasihole state. The expectation values for α larger than one increase very drastically with α since the corresponding natural orbits contain strong components with high momenta as can be seen from the radial shapes in figure 2.

Concluding this part of the discussion we find that the natural orbits with α larger than 1 (indicating their small occupations) represent the high momentum components in the single-particle density and originate mainly from the imaginary part of the Green function at very negative energies. This means that the features of these natural orbits might be explored by analyzing knock-out experiments with large missing energies.

The occupation probabilities and expectation values listed in table IV can also be used to calculate the total energy of the nucleus ^{16}O via the “Koltun sum rule”

$$\mathcal{E} = \sum_{lj} 2 * (2j + 1) \left[\sum_{\Upsilon} \frac{Z_{\Upsilon lj}}{2} \left(\epsilon_{\Upsilon lj}^{qh} + t_{\Upsilon lj}^{qh} \right) + \sum_{\alpha} \frac{n_\alpha^c}{2} (\omega_{lj\alpha} + t_{lj\alpha}) \right] \quad (29)$$

The quasihole contribution to the total energy is calculated in terms of the quasihole energy $\epsilon_{\Upsilon lj}^{qh}$ (see Eq.(20)), the kinetic energy for the quasihole states $t_{\Upsilon lj}^{qh}$ and the spectroscopic factors $Z_{\Upsilon lj}$ (see Eq.(22)). It is remarkable that this quasihole contribution yields only around 37 percent of the total energy although the quasihole part of the single-particle density is responsible for 89 percent of the total particle number. The largest contribution to the energy

in Eq.(29) originates from the continuum part of the natural orbits with $\alpha = 1$. These states contribute more than 58 percent of the total energy although the particle number of these contributions is only around 9 percent. The remaining part of the total energy \mathcal{E} , which is -3 MeV out of the total calculated $\mathcal{E} = -81.1\text{MeV}$ (see also [27]), is due to the natural orbits with α larger than 1.

It is worth repeating that a large part of the density matrix can be described in terms of one natural orbit for each partial wave. These contributions of the $\alpha = 1$ natural orbits account for 97.9 percent of the total particle number and for 96 percent of the total energy. Therefore the description of the single-particle density matrix in terms of these natural orbits with largest occupation probabilities should be sufficient for the calculation of many single-particle observables. It should be kept in mind that already this description in terms of one natural orbit in each partial wave is beyond the mean-field approximation: (i) It allows for a depletion of orbits, which are completely occupied in the mean-field approach, and occupation of partial waves, which are not occupied in the mean-field picture. (ii) This approach takes into account the most important part of the spectral distribution of the single-particle density matrix (see the contributions to the energy in Eq.(29)). The restriction to the natural orbits with $\alpha=1$, however, should not be sufficient to obtain a reliable description of the high-momentum components in the single-particle density matrix. These components are described mainly in terms of the natural orbits with smaller occupation probability.

IV. CONCLUSIONS

Properties of the correlated wave function for the nucleus ^{16}O , which includes the effects of short-range correlations derived from a realistic NN interaction by means of the Green function method [27], have been analyzed in terms of natural orbits. It turns out that the single-particle density matrix can very well be described in terms of a few natural orbits for each partial wave lj . If one restricts the representation of the density matrix in Eq.(1) to only one orbit per partial wave (the orbit with largest occupation probability n_α , here referred to as the $\alpha = 1$ natural orbits), one obtains a density matrix, which accounts already for 97.9 percent of the total particle number. These $\alpha = 1$ natural orbits have a large overlap with the wave functions of the quasihole states as well as the Hartree-Fock (HF) single-particle wave functions for those orbits, which are occupied within the mean-field approximation.

At first sight also the natural orbits in partial waves, which are unoccupied in the HF approximation, and the natural orbits with small occupation probabilities ($\alpha > 1$) look like single-particle wave functions for a nucleons in an excited state of a single-particle potential. A closer inspection shows, however, that the radii for these “excited” orbits are much smaller than those obtained for a motion within a single-particle orbit. These $\alpha > 1$ natural orbits mainly originate from the single-particle Green function at large negative energies ($E < -100$ MeV). Although the occupation of these orbits is much smaller than those with $\alpha=1$, these orbits describe the high-momentum components of the single-particle density matrix. Therefore in order to study these “excited” natural orbits or the high-momentum components of the single-particle density, one has to analyze nucleon knock-out experiments with large missing energy.

For the understanding of the bulk properties of nuclei, like binding energy and radius, it seems to be a good approximation to restrict the study to natural orbits with maximal occupation probability. It is not sufficient, however, to restrict the evaluation of the energy according to the “Koltun sum rule” (Eq.29) to the contributions of the quasihole states. The main contributions arise from the single-particle Green function at energies deep in the 2h1p continuum. In order to improve the present studies towards a self-consistent treatment of the single-particle Green function, it should be a good approximation to describe this Green function in terms of the natural orbits with largest occupation probabilities.

This research project has partially been supported by SFB 382 of the ”Deutsche Forschungsgemeinschaft”, DGICYT, PB92/0761 (Spain), the EC-contract CHRX-CT93-0323, and the U.S. NSF under Grant No. PHY-9307484. One of us (H.M.) is pleased to acknowledge the warm hospitality at the Facultat de Fisica, Universitat de Barcelona, and the support by the program for Visiting Professors of this University.

-
- [1] M. Jaminon, C. Mahaux, and H. Ngô, Phys. Lett. **158 B** (1985) 103
 - [2] L. Lapikas, Nucl. Phys. **A553** (1993) 297c
 - [3] I. Bobeldijk et.al., Phys. Rev. Lett. **73** (1994) 2684
 - [4] K.I. Blomqvist et.al., Phys. Lett. **344 B** (1995) 85
 - [5] H. Morita and T. Suzuki, Prog. Theo. Phys. **86** (1991) 671
 - [6] C. Ciofi degli Atti, E. Pace, and G. Salmè, Phys. Lett. **141 B** (1984) 14

- [7] O. Benhar and V.R. Pandharipande, Phys. Rev. **C47** (1993) 2218
- [8] S.C. Pieper, R.B. Wiringa, and V.R. Pandharipande Phys. Rev. **C 46** (1992) 1741
- [9] Z.Y. Ma and J. Wambach, Phys. Lett. **B 256** (1991) 1
- [10] C. Mahaux and R. Sartor, Adv. Nucl. Phys. **20** (1991) 1.
- [11] A. Ramos, A. Polls, and W.H. Dickhoff, Nucl. Phys. **A503** (1989) 1
- [12] O. Benhar, A. Fabrocini, and S. Fantoni, Nucl. Phys. **A505** (1989) 267.
- [13] C. Ciofi degli Atti, S. Simula, L.L. Frankfurt, and M.I. Strikman, Phys. Rev. **C44** (1991) R7
- [14] B.E. Vonderfecht, W.H. Dickhoff, A. Polls, and A. Ramos, Nucl. Phys. **A 555** (1993) 1.
- [15] C.C. Gearhart, W.H. Dickhoff, A. Polls, and A. Ramos, to be published.
- [16] M. Baldo, I. Bombaci, G. Giansiracusa, U. Lombardo, C. Mahaux, and R. Sartor, Phys. Rev. **C41** (1990) 1748
- [17] H.S. Köhler, Nucl. Phys. **A537** (1992) 64
- [18] S. Stringari, M. Traini, and O. Bohigas, Nucl. Phys. **A516** (1990) 33
- [19] I. Sick, A. Fantoni, A. Fabrocini, and O. Benhar, Phys. Lett. **B 323** (1994) 267
- [20] O. Benhar, A. Fabrocini, S. Fantoni, and I. Sick, Nucl. Phys. **A579** (1994) 493
- [21] D. Van Neck, A.E.L. Dieperink, and E. Moya de Guerra, preprint 1994, nucl-th@xxx.lanl.gov:9410019
- [22] P.-O. Löwdin, Phys. Rev **97** (1955) 1474
- [23] A.N. Antonov, P.E. Hodgson, and I.Zh. Petkov, “*Nucleon Momentum and Density Distributions in Nuclei*” (Clarendon Press, Oxford 1988)
- [24] M.V. Stoitsov, A.N. Antonov, and S.S. Dimitrova, Phys. Rev. **C 48** (1994) 74
- [25] D. Van Neck, M. Waroquier, and K. Heyde Phys. Lett. **B 314** (1993) 255
- [26] H. Müther and W.H. Dickhoff, Phys. Rev. **C 49** (1994) R17
- [27] H. Müther, A. Polls and W.H. Dickhoff, preprint 1994, nucl-th@xxx.lanl.gov:9411005
- [28] R. Machleidt, Adv. Nucl. Phys. **19** (1989) 1.
- [29] W.H. Dickhoff and H. Müther, Rep. Prog. Phys. **55** (1992) 1947.
- [30] D. Bonatsos and H. Müther, Nucl. Phys. **A496** (1989) 23.
- [31] C. W. Wong and D. M. Clement, Nucl. Phys. **A183** (1972) 210.
- [32] K.W. Schmid, H. Müther, and R. Machleidt, Nucl. Phys. **A 530** (1991) 14.
- [33] H. Müther, Prog. Part. Nucl. Phys. **17** (1986) 97
- [34] M. Borromeo, D. Bonatsos, H. Müther, and A. Polls, Nucl. Phys. **A539** (1992) 189.
- [35] M.G.E. Brand, G.A. Rijsdijk, F.A. Muller, K. Allaart, and W.H. Dickhoff, Nucl. Phys. **A531** (1991) 253.
- [36] G.A. Rijsdijk, K. Allaart, and W.H. Dickhoff, Nucl. Phys. **A550** (1992) 159.
- [37] H. Müther and L.D. Skouras, Phys. Lett. **306 B** (1993) 306.
- [38] H. Müther and L.D. Skouras, Nucl. Phys. **A581** (1995) 247
- [39] D. S. Lewart, V. R. Pandharipande, and S. C. Pieper, Phys. Rev. **B37** (1988) 4950.

TABLE I. Occupation of natural orbits in ^{16}O . Listed are the occupation probabilities n_α (see eq.1) of those 4 natural orbits, which show the largest occupation probabilities in various partial waves. Also given are the total occupation probabilities, i.e. the sum over all n_α including orbits with $\alpha > 4$.

α	$s_{1/2}$	$p_{3/2}$	$p_{1/2}$	$d_{5/2}$	$d_{3/2}$	$f_{7/2}$
1	0.9206	0.9467	0.9304	0.0154	0.0189	0.0056
2	0.0127	0.0073	0.0083	0.0033	0.0045	0.0013
3	0.0024	0.0014	0.0019	0.0007	0.0010	0.0003
4	0.0004	0.0003	0.0004	0.0001	0.0001	0.0000
$\sum_\alpha n_\alpha$	0.936	0.956	0.941	0.0195	0.0245	0.0073

TABLE II. Radii of Natural Orbits. Listed are the expectation values of r^2 for natural orbits with largest occupation probabilities in various partial waves. Also given are the expectation value for the total single-particle density ($\langle r^2 \rangle_{lj}$, see Eq. (25)) in each partial wave (normalized to 1) and the corresponding results for the Hartree-Fock (HF) and the quasihole states (qh). All entities listed are given in fm^2 .

α	$s_{1/2}$	$p_{3/2}$	$p_{1/2}$	$d_{5/2}$	$d_{3/2}$	$f_{7/2}$
1	4.092	7.159	7.535	5.746	5.967	6.270
2	4.446	5.761	6.070	7.033	7.215	9.070
3	6.978	9.981	10.364	14.105	13.563	16.296
4	17.982	20.445	20.172	22.776	22.872	26.877
$\langle r^2 \rangle_{lj}$	4.112	7.155	7.534	6.370	6.582	7.392
HF	3.974	7.435	7.963			
qh	4.164	7.258	7.653			

TABLE III. Occupation probabilities for natural orbits obtained by diagonalizing the continuum part of the density matrix for the $l = 0$ partial wave. Results are presented restricting the energy integral of Eq.(19) to the intervals shown in the first line.

α	$[-100\text{MeV}, \epsilon_F]$	$[-\infty, -100\text{MeV}]$	$[-\infty, \epsilon_F]$
1	0.09390	0.04920	0.14118
2	0.00465	0.00627	0.01232
3	0.00058	0.00121	0.00222
4	0.00006	0.00018	0.00037
$\sum_{\alpha} n_{\alpha}$	0.09919	0.05693	0.15612

TABLE IV. Expectation of natural orbits in various partial waves l_j . Listed are the part of the occupation probabilities arising from the quasihole (n_α^{qh}) and the continuum (n_α^c) contribution to the single-particle density, the mean value for the energy ($\omega_{l_j\alpha}$, see Eq.(27)) and the kinetic energy ($t_{l_j\alpha}$, Eq.(28)) in the 2h1p continuum. Furthermore we also give the single-particle energy (ϵ^{qh}) and the kinetic energy t^{qh} of the quasihole states, if they exist.

α	n_α^{qh}	n_α^c	$\omega_{l_j\alpha}$ [MeV]	$t_{l_j\alpha}$ [MeV]
		$s_{1/2}$	$\epsilon^{qh} = -34.30$ MeV, $t^{qh} = 11.23$ MeV	
1	0.77988	0.14068	-87.13	12.49
2	0.00006	0.01268	-118.22	50.28
3	0.00002	0.00234	-126.71	95.49
		$p_{3/2}$	$\epsilon^{qh} = -17.90$ MeV, $t^{qh} = 18.06$ MeV	
1	0.91420	0.03251	-87.22	23.70
2	0.00009	0.00718	-122.75	64.32
3	0.00001	0.00139	-126.26	98.74
			$d_{5/2}$	
1		0.01539	-95.65	44.44
2		0.00332	-115.89	89.77
3		0.00073	-128.97	143.07

FIG. 1. Graphical representation of the Hartree-Fock (a), the 2-particle 1-hole (2p1h, b) and the 2-hole 1-particle contribution (2h1p, c) to the self-energy of the nucleon

FIG. 2. The radial shape of natural orbits with $l_j = s_{1/2}, p_{3/2}$ and $d_{5/2}$. Ordered with respect to the occupation number, results are displayed for $\alpha = 1$ (solid line), 2 (long dashes) and 3 (short dashes)

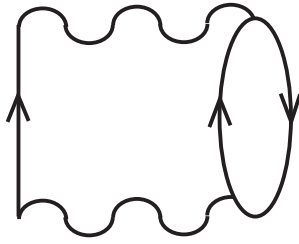
FIG. 3. Orbital shape of the natural orbit ($\alpha = 1$, solid line) the Hartree-Fock (short dashes) and the quasihole wave function in the $s_{1/2}$ partial wave

FIG. 4. Density distribution of nucleons in ^{16}O as a function of the distance r from the center of the nucleus. The result obtained in the HF approximation (long dashes) is compared to the one obtained within the Green function approach (solid line). Also displayed are the contributions of the quasi-hole states to this total density (dash-dotted line) and the density originating from the occupation of states with l larger than 1 (short dashes).

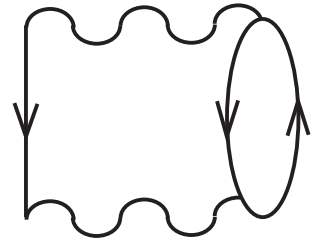
FIG. 5. Natural orbits resulting from the diagonalization of the continuum contribution to the single-particle density in $l = 0$ partial wave. The natural orbits obtained from the energy interval $[-100\text{MeV}, \epsilon_F]$ in Eq.(19) (short dashes) and those from the interval $[-\infty, -100\text{MeV}]$ (long dashes) are compared to those from the whole energy range (solid line). The left part of the figure shows the natural orbits with $\alpha = 1$, while the right part displays those for $\alpha = 3$.



(a)

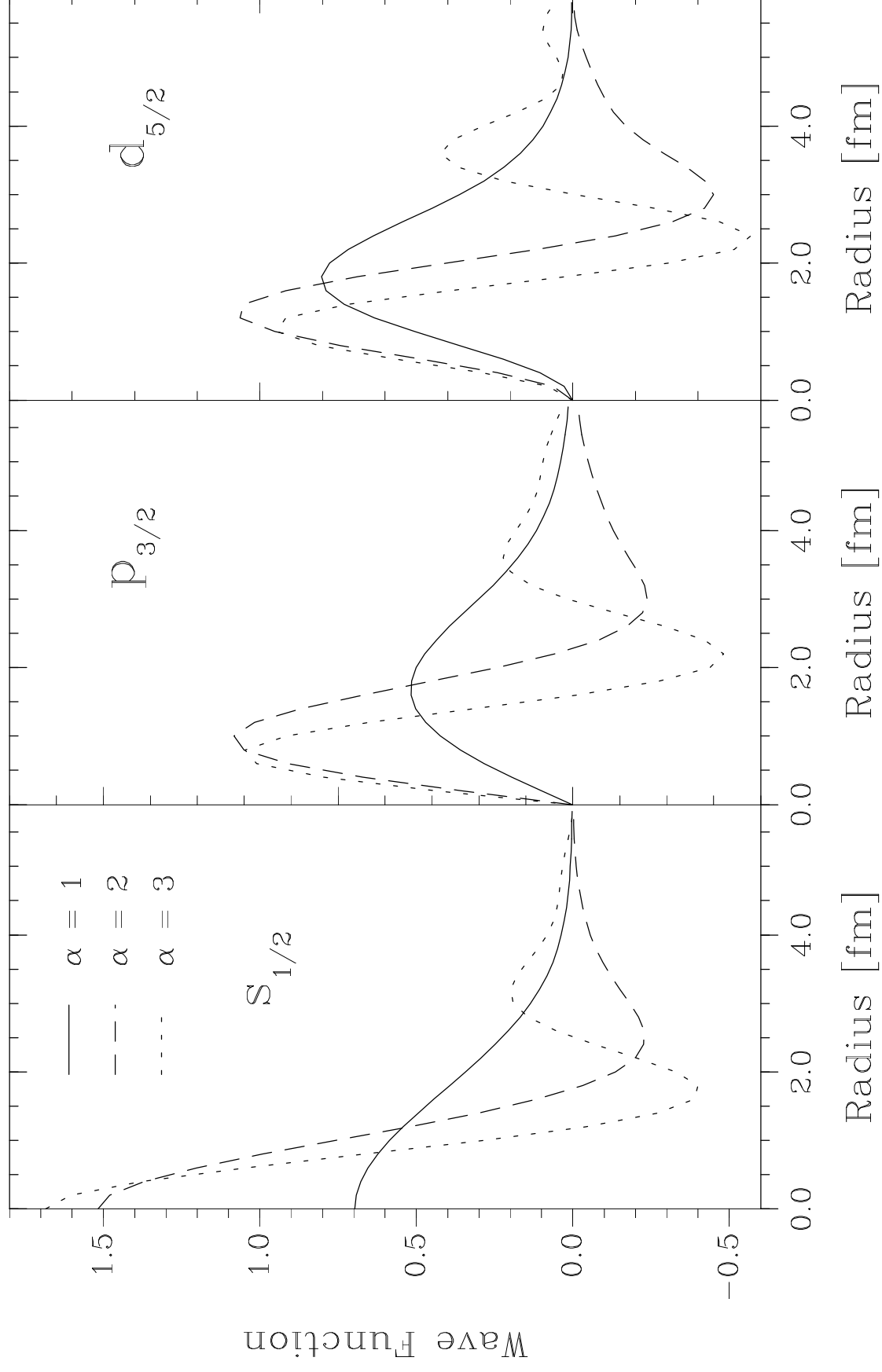


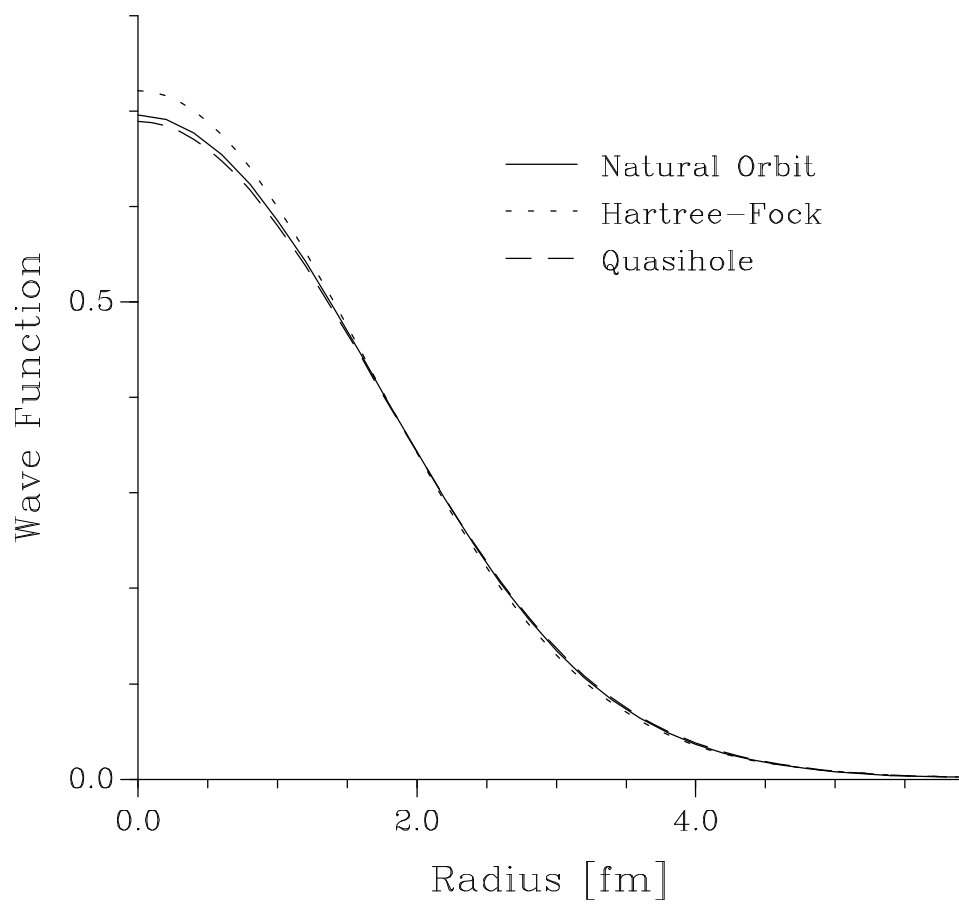
(b)



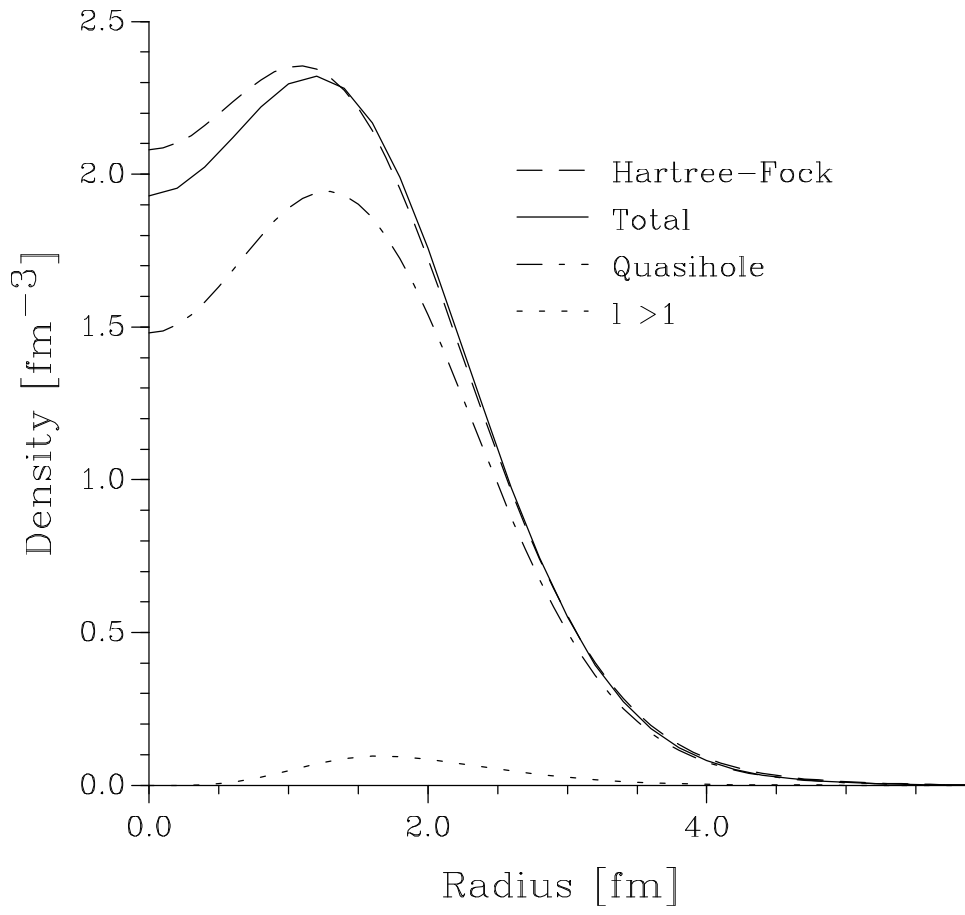
(c)

Natural Orbits





Density Distribution for ^{16}O



Natural Orbits at various Energies

